Simulating the Electronic Structure of Spin Defects on Quantum Computers

Benchen Huang,[1] Marco Govoni,[2,3,*] and Giulia Galli[1,2,3,†]

[1] *Department of Chemistry, University of Chicago, Chicago, Illinois 60637, USA*

[2] *Pritzker School of Molecular Engineering, University of Chicago, Chicago, Illinois 60637, USA*

[3] *Materials Science Division and Center for Molecular Engineering, Argonne National Laboratory, Lemont, Illinois 60439, USA*

(Received 7 December 2021; revised 27 January 2022; accepted 8 February 2022; published 10 March 2022)

We present calculations of both the ground- and excited-state energies of spin defects in solids carried out on a quantum computer, using a hybrid classical-quantum protocol. We focus on the negatively charged nitrogen-vacancy center in diamond and on the double vacancy in 4*H* SiC, which are of interest for the realization of quantum technologies. We employ a recently developed first-principles quantum embedding theory to describe point defects embedded in a periodic crystal and to derive an effective Hamiltonian, which is then transformed to a qubit Hamiltonian by means of a parity transformation. We use the variational quantum eigensolver (VQE) and quantum subspace expansion methods to obtain the ground and excited states of spin qubits, respectively, and we propose a promising strategy for noise mitigation. We show that by combining zero-noise extrapolation techniques and constraints on electron occupation to overcome the unphysical-state problem of the VQE algorithm, one can obtain reasonably accurate results on near-term-noisy architectures for ground- and excited-state properties of spin defects.

DOI: 10.1103/PRXQuantum.3.010339

I. INTRODUCTION

Quantum simulations of the physical and chemical properties of molecules and solids [1–5] are crucial to gain insight into a wide range of complex problems, for example, catalytic reactions [6–8] and the search for optimal materials for sustainable energy sources [9] and quantum technologies [10,11]. One of the essential ingredients of quantum simulations is the solution of the electronic structure problem for molecules and solids, namely the time-independent Schrödinger equation of interacting electrons in the field of atomic nuclei. Such a solution provides the basis for the evaluation of numerous ground- and excited-state properties of matter. However, the algorithms used at present on classical computers to solve the electronic structure problem, especially those based on wave-function methods, face serious computational bottlenecks due to the exponential growth of the dimension of the many-body wave function as a function of the system size [12].

Quantum computers hold promise to drastically improve our ability to carry out quantum simulations of many-electron systems by taking advantage of superposition and entanglement principles offered at the hardware level by quantum bits (qubits) [12–14]. N qubits can represent 2^N complex numbers, which would require 2^{N+7} bits to be represented in double precision on classical computers, and some problems, such as the solution of the Schrödinger equation, may benefit from the memory scaling. Whether one can achieve quantum advantage in solving useful chemistry and physics problems on quantum computers is still under debate. However, efforts to develop algorithms to simulate molecules and solids on quantum computers [15–48] have been flourishing in the past decade and several interesting results on ground and excited states of small molecular systems (containing up to a dozen atoms) have appeared in the literature [15–34].

The number of degrees of freedom and hence the number of atoms that can be handled at present on near-intermediate-scale quantum (NISQ) computers is limited, due to the availability of hardware architectures with only a small number of low-fidelity qubits (a 127-qubit device has recently been announced [49] but the devices used for most calculations that have appeared in the literature have a few tens of qubits). In particular, the hardware limitation poses a challenge for quantum simulations of heterogeneous solids, which require the use of supercells with hundreds of atoms. Recent studies have focused on

*mgovoni@anl.gov

†gagalli@uchicago.edu

two fronts: (i) reducing the complexity of the simulations of condensed phases by using an effective Hamiltonian to represent a fragment (or active part) of a solid [43,50], thus effectively reducing the number of degrees of freedom; and (ii) developing techniques to mitigate the noise present in NISQ hardware [51], which affects the results of calculations on quantum computers. These techniques are based on different methods, including zero-noise extrapolation (ZNE) [52–55], symmetry verification [56], quasiprobability methods [53,54], or stochastic error mitigation [57]. An alternative strategy to complexity reduction is the use of model Hamiltonians, e.g., Hubbard, Heisenberg [35–44], or tight-binding Hamiltonians [45–47].

Recently, we have proposed a computational framework [58] to carry out the calculation of the electronic structure of an active site in a periodic system using a quantum embedding theory that we call here the quantum *defect* embedding theory (QDET) [50,59], which is suitable, for example, for the study of spin defects. Spin defects in semiconductors and insulators are promising candidates for the realization of quantum technologies [11,60–62], including quantum sensing and communication. The electronic states of spin defects usually exhibit a multireference nature, which requires methods beyond mean-field theories for a proper description.

In this work, we present calculations of both ground and excited states of two spin defects, i.e., the nitrogen-vacancy (N-V^-) center in diamond and the double vacancy (hh) configuration (VV) in 4H SiC described by the QDET using a hybrid classical-quantum protocol on a real quantum computer. To the best of our knowledge, the calculations of the excited state are reported here for the first time. In addition, we present the application of a correction scheme to impose physical constraints on the output of quantum simulations and we propose an extrapolation strategy to carry out error mitigation.

The rest of the paper is organized as follows. In Sec. II, we present the classical and quantum algorithms used in this work and in Sec. III the results of our calculations, including error analysis and mitigation techniques. Section IV concludes the paper with a summary and outlook.

II. METHODS

As mentioned in Sec. I, there are numerous problems in condensed-matter physics and chemistry, including point defects in semiconductors, that can be naturally formulated in terms of active regions surrounded by a host medium. These problems can be addressed using embedding theories [50,59,63–69], where the electronic structure of the host and the active region are described at different levels of theory; in particular, a higher level of theory is chosen for the active region, which can describe the multireference character of wave functions. The QDET proposed in Refs. [50,59,67] is an example of embedding theories formulated in terms in Green's functions and it has been shown to accurately describe the low-lying excitations of several spin defects in insulators [50]. The computational strategy of our work is centered on the QDET and on calculations of the electronic structure of spin defects on quantum computers. Figure 1 summarizes the methods

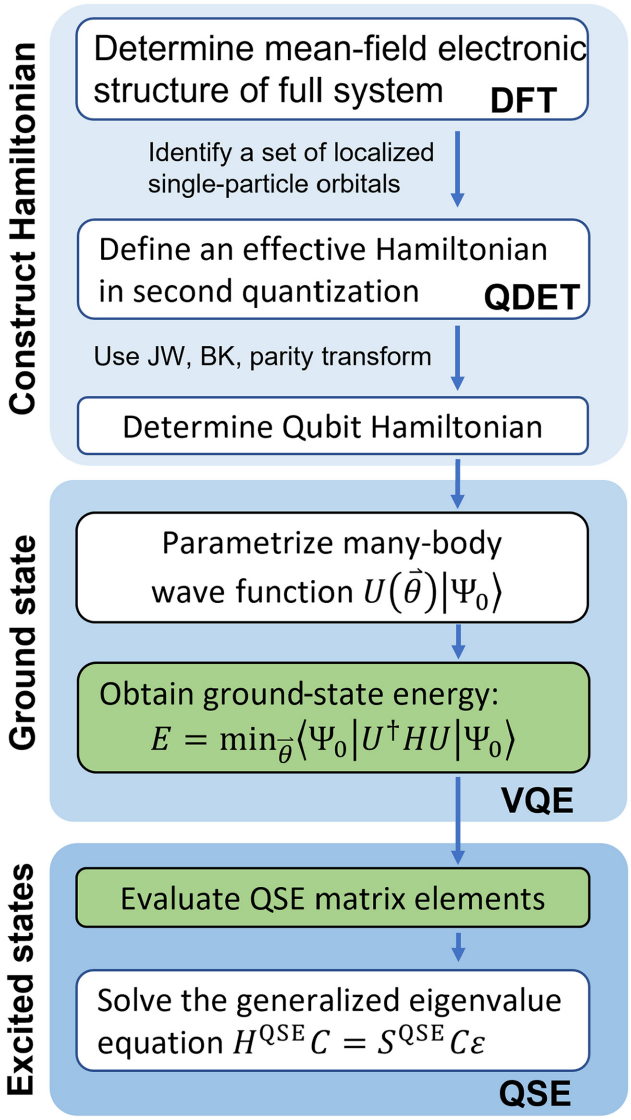

FIG. 1. The work flow used to simulate the ground- and excited-state energies of spin defects, with operations executed on a quantum computer indicated in green. The transformation from a second quantized to a qubit Hamiltonian may be obtained with a Jordan-Wigner (JW), Bravyi-Kitaev (BK), or parity transformation. DFT and QDET denote calculations carried out using density functional theory and the quantum defect embedding theory, respectively. VQE and QSE denote the variational quantum eigensolver and quantum subspace expansion algorithms used for ground- and excited-state calculations, respectively. See the text for definition of the equations.

adopted in this work to carry out mean-field calculations for a chosen supercell, followed by QDET calculations for a defect and the definition of an effective Hamiltonian for the active space of the defect. The calculations of the ground and excited states of the effective Hamiltonian are carried out on a quantum computer with a variational quantum eigensolver (VQE) and the quantum subspace expansion (QSE) algorithm, respectively. These methods, starting with the QDET, are briefly summarized below.

A. Quantum defect embedding theory to obtain effective Hamiltonians

We first define a periodically repeated arrangement of several hundreds of atoms (or a supercell) representing the point defect of interest within a given solid and we compute the electronic structure of the supercell from first principles with density functional theory (DFT) or hybrid DFT. We then select a subset of single-particle wave functions that are localized around the defect and physically represent its electronic states. This subset defines an active space the excitations of which are described by an effective Hamiltonian H_{eff}. The effective potential entering H_{eff} is evaluated by computing the effect of the environment on the active space with many-body perturbation theory techniques; two-body interactions are evaluated using constrained DFT either within the constrained random-phase approximation (cRPA) [70–72] or by explicitly including exchange-correlation effects [73,74]. The effective Hamiltonian includes correlation effects between the electronic states of the active space. In this work, we use the QDET to describe strongly correlated electronic states of point defects that are not properly described by single-determinant wave functions, and hence by DFT.

In essence, using the QDET one can reduce the complexity of evaluating many-body states of a small guest region embedded in a large host system: the problem is reduced to diagonalizing a many-body Hamiltonian simply defined on an active space, where the number of degrees of freedom is smaller than that required to describe the entire supercell of hundreds of atoms.

The active spaces of the systems discussed in this work contain fewer than ten electrons and H_{eff} can be solved using the full-configuration-interaction (FCI) [75] method on a classical computer. However, the FCI scales exponentially with the system size and it has so far been limited to active spaces with up to 22 electrons and 22 orbitals [76], although results of adaptive-sampling CI have been reported for 52 electrons and 52 orbitals [77]. Hence, in order to solve more complex problems, the opportunity offered by quantum computers appears worth exploring, as the overall scaling of FCI may eventually be overcome with quantum architectures.

B. Variational quantum eigensolver to obtain ground-state energies

As mentioned in Sec. I, quantum computers have an exponential memory advantage over classical hardware, which in principle may be harnessed to compute the eigenstates of a fermionic Hamiltonian representing a many-body system of electrons. For example, the quantum-phase-estimation (QPE) [15] algorithm has been proven to be exponentially faster in finding eigenvalues of unitary operators than any available algorithm on a classical computer [78–80]. However, calculations using the QPE are still impractical in the absence of error correction and require quantum resources that exceed the current capability of NISQ hardware [81]. An alternative algorithm to the QPE is the VQE [82], where the properties of many-body states are measured on a quantum device but the parameters that define such states are stored on a classical computer. Therefore, the VQE allows one to use shallower circuits than the QPE and hence to perform calculations on non-fault-tolerant quantum computers [83].

In the past decade, the VQE has been successfully applied to several quantum chemistry problems [16–18,20,26–29,44,82,84–88], including the calculation of the total energies of small molecules [16–18,20,26–29,82], the evaluation of forces by finite differences from Hartree-Fock total energies for the H_2 molecule [84], calculations of the zero-field NMR spectrum of the methyl group of acetonitrile on a trapped-ion quantum computer [85], and calculations of the Heisenberg spin systems using a generalization of the VQE for thermal states [87].

When using the VQE, the ground state of the Hamiltonian is approximated by a normalized trial state $|\Psi(\vec{\theta})\rangle = U(\vec{\theta})\,|\Psi_0\rangle$, where the unitary operator $U(\vec{\theta})$ is constructed using a set of classical parameters $\vec{\theta} = (\theta_1, \ldots, \theta_n)$ and $|\Psi_0\rangle$ is a (usually unentangled) initial state. The expectation value $\langle E(\vec{\theta})\rangle = \langle\Psi(\vec{\theta})|\,\hat{H}\,|\Psi(\vec{\theta})\rangle$ provides an upper bound to the ground-state energy of the system. The energy-expectation value is optimized on a classical computer by variationally optimizing the parameters $\vec{\theta}$, with all inputs (energy values) evaluated on a quantum computer. Here, we use the VQE to find the ground-state energy and corresponding eigenvector of effective Hamiltonians obtained using the QDET.

The physical Hamiltonian (H_{eff}) is mapped onto a qubit Hamiltonian $\hat{H}_q$, e.g., by using the Jordan-Wigner [89], Bravyi-Kitaev [90], or parity [91] mapping: $\hat{H}_q = \sum_i g_i \hat{P}_i$, where g_i are coefficients determined by one- and two-electron integrals and $\hat{P}_i = \{I, X, Y, Z\}^{\otimes N}$ are Pauli correlators acting on N qubits. In general, the mapping from H_{eff} to $\hat{H}_q$ does not ensure that the Hilbert space of the qubit Hamiltonian is the same as that of the original Hamiltonian and hence it is necessary to impose constraints on the many-body wave function through an ansatz to avoid introducing "unphysical states" in the space of $\hat{H}_q$, i.e., states

that are not present in the Hilbert space of H_{eff}. Furthermore, a proper ansatz should satisfy additional multiple requirements. It is, of course, important to choose variational parameters spanning a manifold of states that can accurately approximate the ground state of the system. In addition, the chosen unitary operator $U(\vec{\theta})$ should be constructed in such a way that it can be implemented with the current capacity of gates and qubit connectivity of NISQ computers. There are two classes of ansatze explored in the literature: hardware-efficient ones, designed specifically by taking into account the hardware characteristics [18], and chemistry-inspired ones. The former class usually enables the use of short-depth quantum circuits at the expense of including a large number of variational parameters, while the chemically inspired ones attempt to minimize the number of variational parameters, leading to the need for deeper circuits.

In this work, we choose the unitary coupled-cluster singles and doubles (UCCSD) ansatz [82,92], which belongs to the chemically inspired class and originates from coupled-cluster theory [75,93,94]. The UCCSD ansatz involves the definition of a unitary operator through the exponential of a coupled-cluster operator that contains pertinent single and double electronic excitations:

$$|\Psi\rangle = e^{\hat{T}-\hat{T}^\dagger}\,|\Psi_0\rangle\,,$$
$$\hat{T} = \sum_{i\in\mathcal{A},a\in\mathcal{V}} \theta_i^a \hat{a}_a^\dagger \hat{a}_i + \frac{1}{4}\sum_{i,j\in\mathcal{A};\ a,b\in\mathcal{V}} \theta_{i,j}^{a,b} \hat{a}_a^\dagger \hat{a}_b^\dagger \hat{a}_j \hat{a}_i, \quad (1)$$

where i,j are occupied single-particle orbitals (belonging to subspace $\mathcal{A}$), a,b are virtual orbitals (belonging to subspace $\mathcal{V}$), $\hat{a}^\dagger, \hat{a}$ are the fermionic creation and annihilation operators, and $\theta_i^a, \theta_{i,j}^{a,b}$ are variational parameters. A straightforward implementation of Eq. (1) is challenging, as the operators describing electronic excitations may not commute. A numerically manageable solution may be obtained by introducing a so-called "Trotterized" version of the unitary operator defining the unitary-coupled-cluster (UCC) ansatz. We consider two electronic excitation operators $\hat{A}$ and $\hat{B}$ that do not commute and the Trotter-Suzuki formula:

$$e^{\hat{A}+\hat{B}} = \lim_{n\to\infty}\left(e^{\frac{\hat{A}}{n}} e^{\frac{\hat{B}}{n}}\right)^n. \quad (2)$$

The evaluation of the right-hand side of Eq. (2) requires large values of n, which is expected not to be practical for NISQ computers, as it would require long circuits. An approximation widely adopted in the literature is to use $n = 1$, i.e., $e^{\hat{A}+\hat{B}} \approx e^{\hat{A}} e^{\hat{B}}$ (the one-step first-order Trotter-Suzuki approximation). Such an approximation introduces an error (a Trotter error) and we note that the ordering of A and B on the right-hand side could have an impact on this error, as discussed in Ref. [95].

C. Quantum subspace expansion to obtain excited-state energies

We now turn to the discussion of the calculations of excited states, for which different algorithms are required. The excited states of a fermionic Hamiltonian may be computed on a quantum computer starting from the output of VQE optimizations by using, e.g., the variational quantum deflation (VQD) [96] or QSE algorithms. The former is a constrained variational approach where a penalty term $\langle\Psi_i|\Psi\rangle$ is added to the energy-expectation value to enforce orthogonality among states. A prerequisite for using the VQD is that the target excited states should be included in the manifold of states spanned by the variational wave function defined by the chosen ansatz; such a requirement is not straightforward to ensure. The QSE is an alternative strategy to the VQD and can be viewed as a quantum analog of the FCI. Once a reference wave function $|\Psi\rangle$ is prepared, a set of expansion operators $\{\hat{O}_i\}$ is chosen, which act on $|\Psi\rangle$ to form a basis given by $\{\hat{O}_i\,|\Psi\rangle\}$, where $\hat{O} \in \{\hat{a}_a^\dagger \hat{a}_i,\ \hat{a}_a^\dagger \hat{a}_b^\dagger \hat{a}_j \hat{a}_i | i,j \in \mathcal{A};\ a,b \in \mathcal{V}\}$. We evaluate the Hamiltonian and overlap-matrix elements using such a basis:

$$H_{ij}^{\text{QSE}} = \langle\Psi|\,\hat{O}_i^\dagger \hat{H} \hat{O}_j\,|\Psi\rangle\,,\quad S_{ij}^{\text{QSE}} = \langle\Psi|\,\hat{O}_i^\dagger \hat{O}_j\,|\Psi\rangle\,. \quad (3)$$

Using the matrices defined above, we then solve the generalized eigenvalue problem in the well-conditioned subspace given by

$$H^{\text{QSE}} C = S^{\text{QSE}} C \varepsilon, \quad (4)$$

where C is the matrix of eigenvectors and ε is the diagonal matrix of eigenvalues. As mentioned in Sec. II B, the fermion-to-qubit mapping is used to transform the fermion operators $\hat{a}_i^\dagger, \hat{a}_j$ into Pauli operators acting on N qubits and the matrix elements are evaluated as weighted sums of the expectation values of Pauli correlators. The reference $|\Psi\rangle$ is usually taken to be the ground state. The effectiveness of the QSE relies on a careful choice of creation and annihilation operators, which should enable the description of the desired excitations.

In our work, we use the QSE to compute excited states for two reasons: (i) the construction of the Hamiltonian H^{QSE} and the overlap-matrix S^{QSE} elements may be carried out using the same quantum circuit as those used for VQE [97,98] calculations of the ground state; and (ii) the procedure does not require additional quantum resources but only additional measurements [99].

III. RESULTS

In this section, we describe the results for the many-body ground and excited states of the N-V^- center in diamond and the VV in 4H SiC obtained using the

IBM QISKIT package [100] on the *ibmq_casablanca* quantum computer. In Appendix C, we report the details of the measurement-error-mitigation procedure [101,102], applied to all the measurements carried out on a quantum computer.

A. Reference results on classical hardware

The single-particle electronic structures of the N-V^- center in diamond and the *VV* in 4*H* SiC are computed with hybrid DFT using 216-atom and 200-atom periodic supercells, respectively. We use the plane-wave pseudopotential method as implemented in the QUANTUM ESPRESSO code [103], dielectric-dependent hybrid functionals (DDH) [104], and a kinetic energy cutoff of 50 Ry. For both systems, the active space contains the single-particle states localized at the defect site and we refer to the use of this active space as the "minimum model," which at present represents the best compromise between accuracy and efficiency (see Fig. 2). We adopt the QDET embedding scheme as implemented in the WEST [105] code and we evaluate the dielectric screening beyond the random-phase approximation by coupling the WEST and QBOX [106] codes, as in Refs. [59,107]. The effective Hamiltonian is diagonalized with the FCI using the PySCF code [108] on a classical hardware and the eigenvalues obtained in this way are considered as reference results for our calculations on a quantum computer. The atomic and electronic structures of the defects studied here, the chosen active spaces, and the FCI results are summarized in Fig. 2.

B. Calculation of the ground state using a quantum computer

The ground state of the effective Hamiltonian constructed for both the N-V^- center in diamond and the *VV* in 4*H* SiC is a $^3A_2$ triplet state. Using the minimum models described above (see Fig. 2), the $m_s = 0$ component may be written as a linear superposition of two Slater

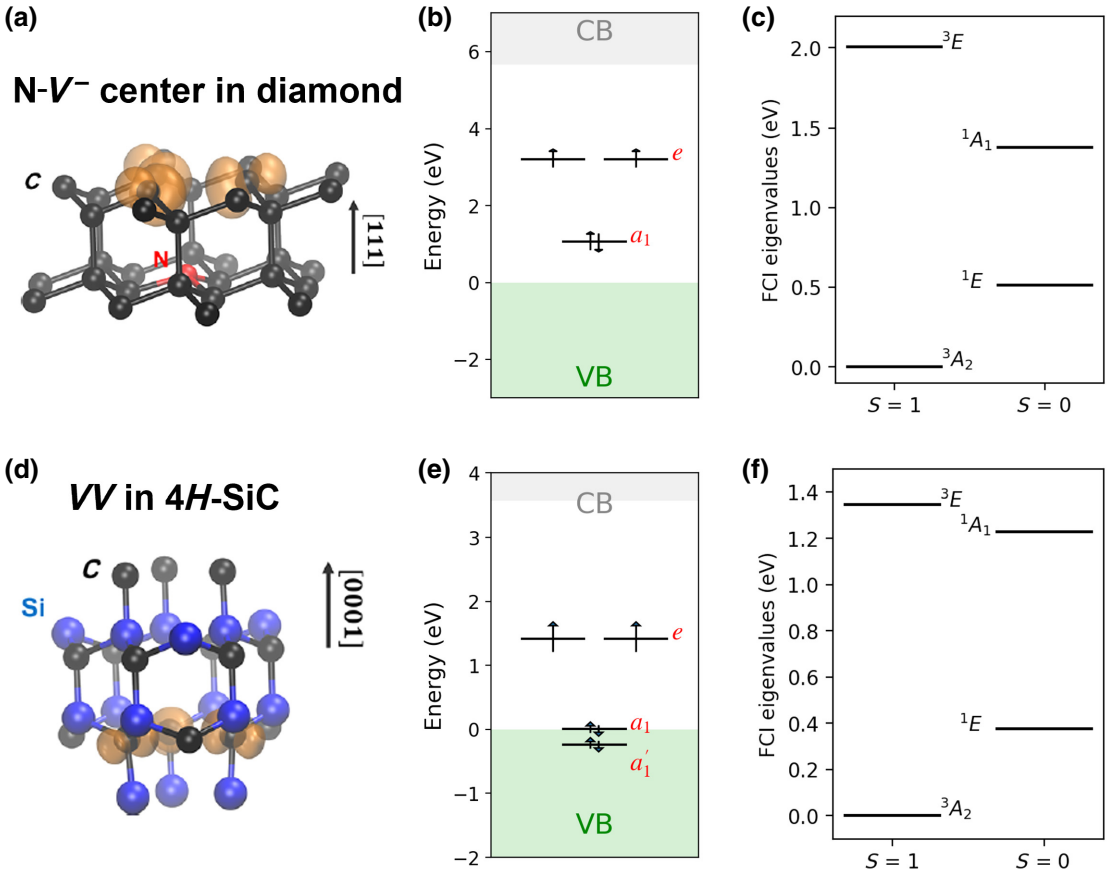

FIG. 2. The spin defects studied in this work: the N-V^- center in diamond and the *VV* in 4*H* SiC. (a),(d) A ball-and-stick representation of the defects, where the orange isosurfaces are the total spin densities. (b),(e) Single-particle states obtained by solving the Kohn-Sham equations for the entire periodic solid, where the gray and green shaded areas represent the conduction band (CB) and the valence band (VB), respectively; the single-particle states shown as black lines are used to build the (4*e*, 3*o*) and the (6*e*, 4*o*) minimum models for the active spaces of the N-V^- and *VV* centers, respectively. (c),(f) The low-lying many-body energy levels obtained by solving the effective Hamiltonians using the FCI method on classical hardware.

determinants [50]:

$$|^3A_2, m_s = 0; \mathrm{N}\,V^-\rangle = \frac{1}{\sqrt{2}}\left(|a_1\bar{a}_1 e_x\bar{e}_y\rangle + |a_1\bar{a}_1\bar{e}_x e_y\rangle\right), \tag{5}$$

$$|^3A_2, m_s = 0; VV\rangle = \frac{1}{\sqrt{2}}\left(|a_1'\bar{a}_1' a_1\bar{a}_1 e_x\bar{e}_y\rangle + |a_1'\bar{a}_1' a_1\bar{a}_1\bar{e}_x e_y\rangle\right), \tag{6}$$

for the N-V^- and the VV center, respectively. In Eqs. (5) and (6), a_1', a_1, e_x, and e_y (spin-up) and $\bar{a}_1'$, $\bar{a}_1$, $\bar{e}_x$, and $\bar{e}_y$ (spin-down) denote the single-particle orbitals.

We first focus on the N-V^- center and consider two initial states that are used as trial wave functions for the VQE algorithm: (a) $|a_1\bar{a}_1 e_x\bar{e}_x\rangle$ or (b) $|a_1\bar{a}_1 e_x\bar{e}_y\rangle$. The UCCSD expression of Eq. (1) is used as an ansatz for the unitary operator applied to the trial state. In case (a), the ansatz leads to a trial wave function with six variational parameters, whereas in case (b), the trial wave function contains only $\theta_{e_x\bar{e}_y}^{e_y\bar{e}_x}$ as variational parameter (for convenience of notation, we refer to this parameter as θ, since all additional parameters may be set to zero to enforce a triplet solution from the start). The effective Hamiltonian of both systems is transformed into a qubit representation using the parity mapping [91].

Figure 3 shows the convergence of the ground-state energy as a function of the number of VQE iterations, starting from either trial state. We obtain convergence to the same results as obtained with the FCI when using a quantum simulator (i.e., in the absence of noise) for both trial states; however, we obtain two different values when using *ibmq_casablanca*, due to the presence of hardware noise. Not surprisingly, the impact of noise on the results depends on the choice of the initial state. In case (a), where there are six variational parameters and the circuit depth is 26, we obtain an approximately 0.07 eV error, while in case (b), where there is only one variational parameter and the circuit depth is 6, the error is smaller (approximately 0.02 eV). For case (b), i.e., when the initial state $|\Psi_0\rangle = |a_1\bar{a}_1 e_x\bar{e}_y\rangle$, the variational wave function in the UCCSD ansatz reads (see Appendix A)

$$|\Psi(\theta)\rangle = \cos\left(\frac{\theta}{2}\right)|a_1\bar{a}_1 e_x\bar{e}_y\rangle + \sin\left(\frac{\theta}{2}\right)|a_1\bar{a}_1\bar{e}_x e_y\rangle\,. \tag{7}$$

As expected, the energy has a minimum when $\theta = \pi/2$, i.e., for $|\Psi(\pi/2)\rangle = |^3A_2, m_s = 0; \mathrm{N}\,V^-\rangle$. In the following, we choose the initial state as in (b) above and use a simultaneous perturbation stochastic approximation (SPSA) [111] optimizer, which has been shown to be robust to noise [18]. The corresponding quantum circuit is depicted in Fig. 4. We choose physical qubits such that the mapping leads to a qubit configuration minimizing faulty controlled-NOT (CNOT) gates (see Appendix C).

The energy obtained with the VQE as a function of the number of iterations is reported in Figs. 5(a) and 5(b) (blue dots). We find that several measurements of the energy yield a value smaller than the FCI result and the number of occurrences is larger for the VV than the N-V^- center. These incorrect results are a manifestation of the so-called unphysical-state problem [112,113], where in some cases quantum circuits yield states with an incorrect number of electrons, causing an inaccurate evaluation of the energy. The unphysical-state problem has been pointed out by Sawaya *et al.* [112], using simple noise models to study second-row dimers and several methods to correct for

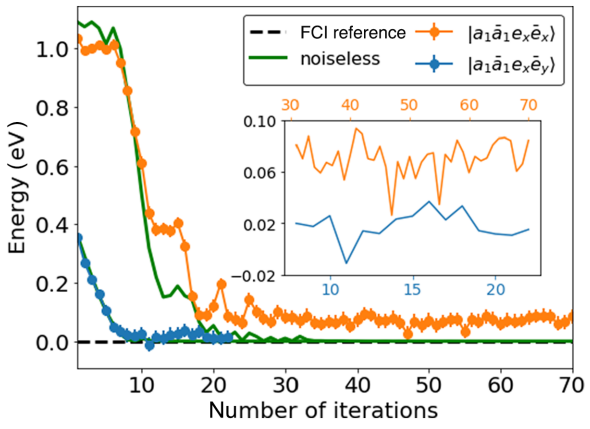

FIG. 3. The optimization of the $|^3A_2, m_s = 0\rangle$ state of the N-V^- center using the VQE on *ibmq_casablanca* and on a noiseless simulator using four qubits. The strongly correlated $\frac{1}{\sqrt{2}}(|a_1\bar{a}_1 e_x\bar{e}_y\rangle + |a_1\bar{a}_1\bar{e}_x e_y\rangle)$ state is obtained starting from the $|a_1\bar{a}_1 e_x\bar{e}_x\rangle$ state or the $|a_1\bar{a}_1 e_x\bar{e}_y\rangle$ state. We use the parity transformation to obtain the qubit Hamiltonian acting on four qubits; the optimization is carried out with the COBYLA algorithm [109]. The noiseless simulation is performed with the QASM simulator [110]. The zero of energy is the result obtained on classical hardware with the FCI method. In the inset, we compare the converged energies obtained from the two chosen trial states.

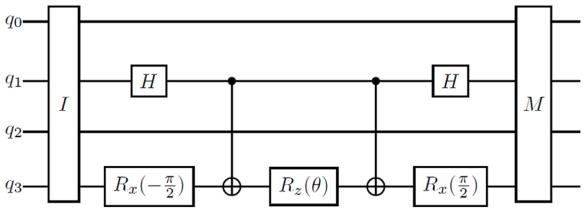

FIG. 4. The quantum circuit executed on four qubits (labeled q_0 to q_3): I and M represent the state initialization and measurement blocks, respectively. The measurement block includes Pauli correlators so as to enable the measurement of observables, e.g., the energy and the electron number. The symbol H represents a Hadamard gate; $R_{x,z}(\theta)$ represents the rotation of the variational parameter θ (see the text) around the x, z axis respectively.

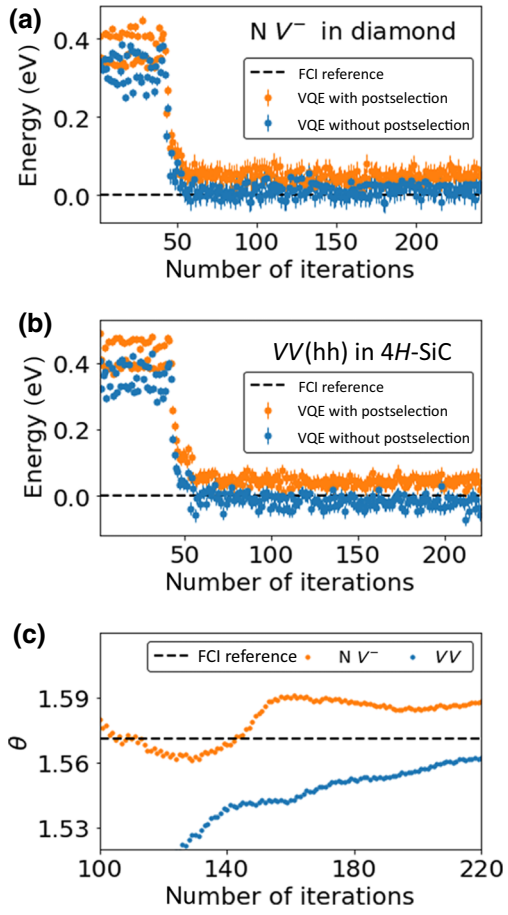

FIG. 5. The optimization of the ground-state energy of (a) the N V^- in diamond and (b) VV in 4H SiC, carried out with the VQE algorithm using four and six qubits, respectively, on *ibmq_casablanca*, with (orange dots) and without (blue dots) postselection of states (see the text). The FCI energy is reported for reference. (c) The variation of the parameter θ [see Eq. (7)] in the VQE optimization; the value is obtained from averaging the parameter at the end of the VQE optimization. The dashed line corresponds to the exact solution, i.e., $\theta = \frac{\pi}{2}$.

unphysical states have recently been proposed, including error detection using ancilla qubits [113].

We find that the apparent violation of the variational principle does pose a serious problem to the applicability of the VQE algorithm to the calculations of the electronic properties of spin defects in materials. The severity of this problem also depends on the chosen fermion-to-qubit transformation, which in turn determines the extent to which the qubit Hilbert space differs from the configuration state space spanned by the fermionic Hamiltonian [114].

We adopt a postselection method to enforce the validity of the variational principle during the VQE optimization. After using the fermion-to-qubit transformation, the energy is evaluated on the quantum hardware as the weighted sum of the expectation values of Pauli correlators, i.e., $E = \sum_i g_i \langle \hat{P}_i \rangle$. The expectation values of all Pauli correlators are obtained by measuring N_c independent circuits 8192 times where N_c is the number of groups of Pauli correlators that contain commuting operators. The number of electrons may be determined simultaneously from the group of operators that only contains diagonal Pauli correlators (those with only I and Z gates) [115]. In our calculations, we discard all measurement outcomes that do not conserve the number of electrons. Interestingly, the weights g_i of the diagonal Pauli correlators lead to the dominant contribution to the energy. The orange curves in Figs. 5(a) and 5(b) show the convergence of the VQE algorithm when energy measurements are obtained with the postselection method and Fig. 5(c) shows the convergence of the variational parameter θ with a relative error of less than 2%. Upon enforcement of the postselection rule, all measured energies turn out to be higher than the reference value for the ground state. Interestingly, the same postselection method has also been adopted in the calculation of the total energy of LiH [115], yielding a notable improvement in the accuracy of energy measurements, with a small overall error of about 1 kcal/mol.

In Fig. 6, we further analyze the effects of noise on the results by scanning the total energy as a function of θ: $E(\theta = \pi/2)$ is the energy of the ground state and $E[\theta = -(\pi/2)]$ that of an excited state. In the region close to the minimum (ground state), the values obtained with postselection (orange curve) are higher than the noiseless reference values (dashed black curve): indeed, the postselection process removes states that, due to the presence of noise, do not correspond to the correct number of electrons; hence, in virtue of the variational principle, one obtains an energy higher than the reference value. However, in the region close to $\theta = -(\pi/2)$ (excited state), where the

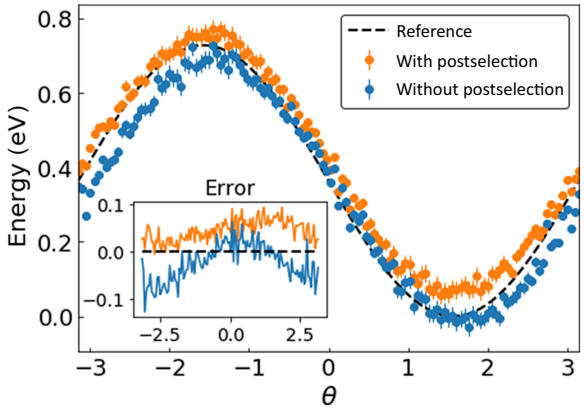

FIG. 6. The energy variation of the ground state of the N-V^- center in diamond as a function of the parameter θ (see Eq. (7) in the text) using *ibmq_casablanca*. We show results with (orange) and without postselection of states (blue). The straight black line (ref) indicates the energy obtained with a noiseless simulator. The inset shows the difference between the energy evaluated on quantum and classical hardware.

variational principle does not hold, even after postselection one may obtain errors of different signs. Therefore, a spurious cancelation of errors may occur and the overall error on the energy for $\theta < 0$ appears to be smaller than in the proximity of the ground state ($\pi/2$).

To improve the accuracy of the energy measurements, numerous mitigation schemes have been developed, including the quasiprobability method [53,54], individual error reduction [116], and learning-based error mitigation [117–120]. These methods require complete information about the noise channel or a large number of quantum measurements. We note that quantum noise is usually described using the language of open quantum systems and Kraus operators and exact forms of these operators [51] are required in order to obtain complete information about the noise channel, which is a difficult task for realistic hardware architectures. Here, we adopt the ZNE method, which is straightforward to implement and does not require additional qubits. The essence of the method is the expansion of the expectation value of an observable—for instance, the energy E–as a power series of noise around its zero-noise value E^* [51,121]:

$$E(\lambda) = E^* + \sum_{k=1}^{n} a_k \lambda^k + O(\lambda^{n+1}). \tag{8}$$

Here, λ is an appropriately small ($\lambda \ll 1$) noise parameter and the coefficients in the expansion a_k depend on specific details of the noise (i.e., on the unknown form of the Kraus operators describing the specific noise channels). The basic idea of the ZNE is to amplify the noise of the circuit to various controllable levels and obtain the zero-noise limit by extrapolation. Error mitigation via the ZNE has been explored in several pioneering papers [121–123] investigating small molecules and Ising Hamiltonians. Popular ways to artificially boost the error include identity insertions [124], unitary folding [125], Pauli twirling [52,126], and rescaling of the Hamiltonian [53,121,127].

Here, we propose a simple technique to boost the error for the ZNE, which we call exponential block replication. The method is applicable to all cases where the UCC or the qubit coupled cluster (QCC) ansatz [128–133] is used. As discussed in Sec. II B, UCC ansatze are typically implemented using the approximation $e^{\hat{A}+\hat{B}} \approx e^{\hat{A}} e^{\hat{B}}$. In this case, multiple consecutive applications of n exponential blocks lead to the following expression: $e^{\hat{A}+\hat{B}} \approx e^{\hat{A}} e^{\hat{B}} = \left[e^{(\hat{A}/n)}\right]^n \left[e^{(\hat{B}/n)}\right]^n$. This expression is different from that obtained with a n-step first-order Trotter decomposition, where $e^{\hat{A}+\hat{B}} \approx \left[e^{(\hat{A}/n)} e^{(\hat{B}/n)}\right]^n$. By adopting this procedure, we successfully increase the overall depth of the circuit by integer multiples of the original block and we artificially amplify the noise level without modifying the expression of the many-body wave function or affecting the Trotter error.

Our extrapolation procedure is shown in Fig. 7. We consider $n = [1, 2, 3, 4, 5]$ and for each value of n we repeat the 8912 measurements of each circuit 50 times (for a total of $50 \times 8912 = 445\,600$ measurements), in order to improve the stability of the extrapolation procedure. Repeating the measurement of each circuit 25 times instead of 50 leads to a small difference of approximately 0.012 meV in the computed energy. The difference between the ground-state energy obtained with 50 repetitions and the reference value obtained on a quantum simulator is approximately 0.002 eV for the N-V^- center and approximately 0.005 eV for the VV in SiC, one order of magnitude smaller than in the case where the ZNE is not applied.

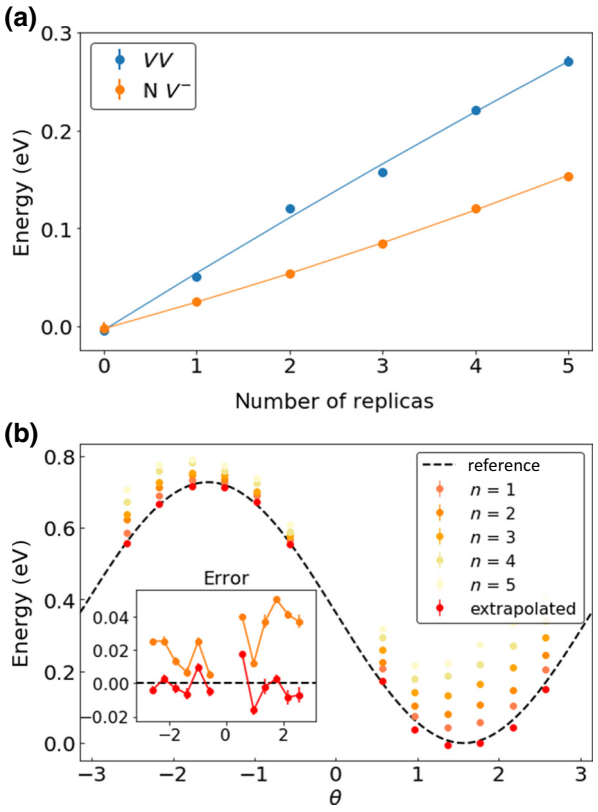

FIG. 7. (a) The ground-state energy of the N-V^- center and the VV in 4H SiC as a function of the number of replicas used in the zero-noise extrapolation (see text). The reference noiseless result is set at 0. (b) The total energy of the N-V^- center as a function of the parameter θ [Eq. (7) in the text]. The different colors correspond to using $n = [1, 2, 3, 4, 5]$ replicas of exponential blocks and the red dots denote the linearly extrapolated energy ($n \to 0$). In the inset, we show the difference between noisy energies ($n = 1$) or extrapolated values ($n \to 0$) and the noiseless reference energy. Both (a) and (b) are obtained using *ibmq_casablanca*.

Figure 7 also shows the results of the ZNE for the energy of the N-V^- center as a function of θ. The extrapolation is performed considering an increasing number of replicas (n) and averaging over 24 repetitions of 8912 measurements for each replica. The choice of 24 instead of 50 repetitions is a compromise between efficiency and accuracy: scanning $E(\theta)$ (i.e., computing 12 values of the energy with a 50-time repetition rate) would require a time to completion during which we could not ensure a constant noise level on the available hardware. Since we show earlier that 25 repetitions yield an acceptable result for the ground state, we use a similar number for the calculation of the function $E(\theta)$. The inset of Fig. 7 shows the difference between noisy results ($n = 1$) and extrapolated values ($n \to 0$) and the noiseless reference. Overall, we see that results obtained with the ZNE are in closer agreement with the reference results. The errors of extrapolation in Fig. 7 are computed using the method discussed in Appendix B.

C. Calculation of the excited states using a quantum computer

We compute excited states of the N-V^- and VV centers using the QSE algorithm. To avoid propagating the errors introduced by the VQE, we use the exact energy of the $^3A_2$ state, with $m_s = 0$ as ground-state energy.

We construct a quantum subspace that is identical to the configuration state space, so the dimension of the QSE matrices is the same as that of their classical FCI counterpart. The QSE matrix is built by evaluating, on the quantum hardware, the expectation values of all Pauli correlators; in addition, we adopt the postselection and ZNE techniques described above. To perform ZNE, we use a linear extrapolation for the off-diagonal elements of the QSE matrix and we compute diagonal elements with linear, quadratic, or exponential extrapolations. The number of repetitions of the same circuit with 8192 measurements is reduced from 50 to 10 for the VV due to the computational cost. The QSE matrix is diagonalized on a classical computer.

The results are summarized in Table I. The accuracy of the energy of nondegenerate excitations is, in general, improved when using the ZNE, with the only exception being the $^3A_2 \leftrightarrow {}^3E$ transition of the N V^- in diamond, obtained using a quadratic extrapolation scheme. We note that, overall, different choices of extrapolation functions lead to similar results and hence linear extrapolation is a desirable choice, since a smaller number of parameters is expected to lead to a more stable fit. Unfortunately, we find that the degeneracy of states is spuriously lifted on the quantum hardware due to the presence of noise, even after applying the ZNE, showing that it is not possible to resolve energy differences smaller than the standard deviation (σ) associated with the mean of our measurements. In our calculations with 50 repetitions, $\sigma \simeq 3$ meV.

IV. CONCLUSIONS

In summary, we present electronic structure calculations of strongly correlated ground states and, for the first

TABLE I. The excitation energies (in electronvolts) of the N-V^- and VV centers calculated using the QSE method. The first column shows transitions between states labeled using the representation of the point group C_{3v}, following Ref. [50]. The second column shows results obtained with a noiseless simulator, which are identical to those of classical FCI calculations on a classical computer. The third to sixth columns display results obtained using the QSE on the quantum hardware and using postselection of states with different extrapolation strategies and the zero-noise extrapolation technique.

	FCI or noiseless	No extrapolation	Linear[a]	Quadratic[b]	Exponential[c]
N-V^- center					
$^3A_2 \leftrightarrow {}^1E$[d]	0.512	0.470	0.511	0.508	0.509
$^1E \leftrightarrow {}^1E$[e]	0.000	0.076	0.074	0.084	0.080
$^3A_2 \leftrightarrow {}^1A_1$	1.380	1.282	1.391	1.373	1.378
$^3A_2 \leftrightarrow {}^3E$[d]	2.008	1.964	1.989	1.946	1.974
$^3E \leftrightarrow {}^3E$[e]	0.000	0.177	0.119	0.059	0.091
VV in SiC					
$^3A_2 \leftrightarrow {}^1E$[d]	0.378	0.338	0.367	0.363	0.365
$^1E \leftrightarrow {}^1E$[e]	0.002	0.083	0.069	0.065	0.067
$^3A_2 \leftrightarrow {}^1A_1$	1.228	1.141	1.212	1.207	1.202
$^3A_2 \leftrightarrow {}^3E$[d]	1.348	1.313	1.337	1.333	1.334
$^3E \leftrightarrow {}^3E$[e]	0.002	0.010	0.080	0.079	0.078

[a]Linear extrapolation of both diagonal and off-diagonal elements of the QSE matrix [Eq. (8) in the text].
[b]Quadratic extrapolation of the diagonal, and linear of the off-diagonal, elements of the QSE matrix.
[c]Exponential extrapolation of the diagonal, and linear of the off-diagonal elements, of the QSE matrix.
[d]The energy of the degenerate states is computed as the average of the two energies obtained on quantum hardware.
[e]The energy gap between two states, which should be degenerate, due to the presence of noise.

time, of excited electronic states of point defects in semiconductors on a near-term quantum computer. We focus on two spin defects, i.e., the N-V^- center in diamond and the VV in SiC. Our computational protocol includes first-principles calculations of the electronic structure of a spin defect in a solid containing hundreds of atoms using hybrid DFT, followed by the use of the quantum defect embedding theory to define an effective Hamiltonian that represents electronic excitations localized within the point defect. The Hamiltonian is then mapped into a qubit Hamiltonian that is solved using the VQE and QSE hybrid classical-quantum algorithms to obtain the ground and excited many-body electronic states of the defect, respectively. We discuss the merits of these algorithms in the case of spin qubits; however, establishing which algorithms are better suited to obtain, in general, many-body energies of electronic states in solids on NISQ hardware remains an open area of research [14]. For example, recent papers have proposed methods to find the eigenstates of a fermionic Hamiltonian that are not based on the variational principle and therefore do not require the definition of an ansatz or involve an optimization procedure [40]. In particular, Ref. [134] has proposed an algorithm to prepare approximate ground states with a shallow circuit and just one parameter.

We also discuss two main problems arising from the presence of noise on quantum hardware: (i) the apparent violation of the variational principle in VQE calculations due to unphysical states arising when the number of electrons is not conserved; and (ii) the presence of persisting errors on energies obtained on quantum computers even after correcting for the presence of unphysical states. We successfully apply a postselection method based on partial constraints on the number of electrons to correct for problem (i) and we propose an error-mitigation technique within the ZNE scheme to reduce the effect of quantum errors. The technique uses an exponential block repetition to boost the quantum error of UCC-type ansatze in a controllable fashion. The error-mitigation protocol adopted here has several advantages: (1) it is readily applicable without any knowledge of the source of hardware noise and without increasing the number of qubits; and (2) it does not affect the scaling of the quantum algorithm, although it may affect the prefactor. However, the UCC-type ansatze require the use of relatively deep circuits, thus limiting the applicability of the ZNE strategies with a large number of replicas. As a proof of principle of the strategies adopted here to solve useful materials problems, we obtain results with small active spaces and shallow circuits. Work is in progress to expand the applicability of the method to systems that require larger active spaces appropriate to investigate, for example, adsorbates on surfaces and ions or nanostructures in solution. Based on our work, we further envision a feedback loop, where quantum simulations of material properties on a quantum device lead to the prediction of new materials and properties for the design of improved quantum computers, which will in turn result in enhanced property predictions and applications, therefore establishing a tight connection between quantum computations and material predictions.

ACKNOWLEDGMENTS

We thank He Ma, Nan Sheng, Christian Vorwerk, Liang Jiang, and Martin Suchara for many fruitful discussions. We also thank the QISKIT Slack channel for generous help. This work was supported by the computational materials science center Midwest Integrated Center for Computational Materials (MICCoM) for the implementation and use of quantum embedding and by the Next Generation Quantum Science and Engineering (QNEXT) hub for the development of quantum algorithms and deployment on quantum hardware. MICCoM is part of the Computational Materials Sciences Program funded by the U.S. Department of Energy, Office of Science, Basic Energy Sciences, Materials Sciences, and Engineering Division through the Argonne National Laboratory, under Contract No. DE-AC02-06CH11357. QNEXT is supported by the U.S. Department of Energy, Office of Science, National Quantum Information Science Research Centers. This research used resources of the Oak Ridge Leadership Computing Facility at the Oak Ridge National Laboratory, which is supported by the Office of Science of the U.S. Department of Energy under Contract No. DE-AC05-00OR22725, resources of the National Energy Research Scientific Computing Center (NERSC), a DOE Office of Science User Facility supported by the Office of Science of the U.S. Department of Energy under Contract No. DE-AC02-05CH11231, and resources of the Argonne Leadership Computing Facility, which is a DOE Office of Science User Facility supported under Contract No. DE-AC02-06CH11357. We acknowledge the use of IBM Quantum services for this work. The views expressed are those of the authors and do not reflect the official policy or position of IBM or the IBM Quantum team.

APPENDIX A: ANSATZ

We discuss the case of the N-V^- center in diamond as an example. We use a ($4e$, $3o$) active space, as shown in Fig. 2. After parity mapping and tapering off qubits, the ground state can be represented as

$$|^3A_2, m_s = 0\rangle = \frac{1}{\sqrt{2}}\left(|011001\rangle + |001011\rangle\right) \xrightarrow{\text{tapering}} \frac{1}{\sqrt{2}}\left(|1101\rangle + |0111\rangle\right), \quad \text{(A1)}$$

where we denote the spin-up orbitals by 0, 1, and 2 and the spin-down orbitals by 3, 4, and 5, in ascending order

of energy. The zeroth and second qubits remain 1 after tapering, since the a_1 orbital is occupied. By selecting only spin-conserving excitations, we are left with one variational parameter, θ_{15}^{24} ($\theta_{e_x\bar{e}_y}^{e_y\bar{e}_x}$), and the operator acting on the initial state may be written as

$$U(\theta_{15}^{24})\,|1101\rangle = e^{-\mathrm{i}\frac{\theta_{15}^{24}}{4}(Y_1X_3 - X_1Y_3)}\,|1101\rangle = e^{\mathrm{i}\frac{\theta_{15}^{24}}{2}X_1Y_3}\,|1101\rangle\,, \tag{A2}$$

where we take advantage of commutation rules [20]. This assumption leads to a simple ansatz circuit similar to that shown in Fig. 4. When running on a quantum simulator, we obtain converged values within 10^{-9} eV.

APPENDIX B: ERROR EXTRAPOLATION

The error in measuring $\langle H\rangle$ has two components: a systematic and a stochastic [82] component. In our extrapolation, we estimate the standard deviation of $\langle H\rangle$ at each number of circuit replicas n. In addition, we estimate the error present in the zero-noise limit. To do so, we conduct 50 repetitions of each measurement of $\langle H(n)\rangle$ and compute an average value $\overline{E}_n$ and distribution σ_E.

Assume $\overline{E}_n$, as a function of the number of replicas n, can be approximated by a polynomial function. $\overline{E}$ may be used for both fitting and extrapolation procedures. Importantly, the error associated with $\overline{E}$ is $\sigma_{\overline{E}} = \sigma_E/\sqrt{N}$, where here N is the number of independent (repeated) measurements. We call the error on $\overline{E}$ in the zero-noise limit $\overline{E}_{\mathrm{obj}} \pm \sigma_{\mathrm{obj}}$.

We first fit the data sets $\{n_i, i = 1\cdots m\}$ and $\{\overline{E_i}, i = 1\cdots m\}$ with a polynomial function. Using a least-squares fit, the function to be determined is parametrized as

$$\overline{E} = \sum_{i=0}^{p} \alpha_i n^i \tag{B1}$$

and the parameters can be obtained by solving the linear system $L\alpha = K$, where

$$L = \begin{bmatrix} m & \sum_{i=1}^m n_i & \cdots & \sum_{i=1}^m n_i^p \\ \sum_{i=1}^m n_i & \sum_{i=1}^m n_i^2 & \cdots & \sum_{i=1}^m n_i^{p+1} \\ \vdots & \vdots & \ddots & \cdots \\ \sum_{i=1}^m n_i^p & \sum_{i=1}^m n_i^{p+1} & \cdots & \sum_{i=1}^m n_i^{2p} \end{bmatrix},$$

$$\alpha = \begin{bmatrix} \alpha_0 \\ \alpha_1 \\ \vdots \\ \alpha_p \end{bmatrix},\quad K = \begin{bmatrix} \sum_{i=1}^m \overline{E_i} \\ \sum_{i=1}^m n_i\overline{E_i} \\ \vdots \\ \sum_{i=1}^m n_i^p\overline{E_i} \end{bmatrix}. \tag{B2}$$

The result briefly reads $\alpha = L^{-1}K$, where each α_i is a linear combination of $\{\overline{E}_i, i = 1\cdots m\}$. α can be expressed as $\alpha = AE$, where A is a $(p+1)\times m$ matrix with entries $\{A_{ij}\}$, and E is a $m\times 1$ matrix with entries $\{\overline{E}_i\}$. The standard deviation of θ, which is a $(p+1)$-dimensional vector, satisfies the following equation:

$$\sigma_\alpha \odot \sigma_\alpha = (A\odot A)(\sigma_{\delta d}\odot\sigma_{\delta d}). \tag{B3}$$

Here, $\sigma_{\overline{E}}$ is not a scalar but a $m\times 1$ matrix with entries $\{\sigma_{\overline{E}_i}\}$. $\odot$ is the Hadamard product. The quantity $\overline{E}_{obj}$ is given by α_0, and we obtain

$$\alpha_0 \pm \sigma_{\alpha_0}. \tag{B4}$$

APPENDIX C: DESCRIPTION OF QUANTUM HARDWARE

We use the *ibmq_casablanca* processor running QISKIT v0.24.1 [100]. The layout of this quantum device is shown in Fig. 8, where the coupling qubits are connected by a solid line. Table II summarizes the coherence time, single-qubit, two-qubit, and readout error rates of the device when the measurements reported in the main text are executed. In choosing the qubit device mappings shown in the main text, preference is given to the qubit pairs with relatively small CNOT error rates. In our experiments, CNOT gates are executed between Q1 and Q3 on the device.

In addition to the errors discussed in the main text, processes involved in state preparation and measurement are noisy as well and these errors are usually denoted as state-preparation-and-measurement (SPAM) errors. To reduce the effect of noise due to final measurement errors, QISKIT recommends a measurement-error-mitigation approach [102]. To do so, we adopt a recommended calibration procedure on the chosen basis states before each measurement of the energies, in order to characterize the device noise. After each calibration measurement, we arrange the results

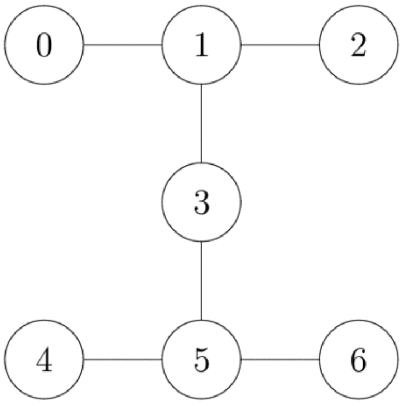

FIG. 8. The seven-qubit *ibmq_casablanca* device layout.

TABLE II. Calibration data for the *ibmq_casablanca* device. T_1 and T_2 denote the coherence time of the qubits. The fourth and fifth columns display the single-qubit X rotation and the readout error rate of each qubit. The last column displays the two-qubit CNOT error rate between the coupling qubit pairs. The CX in the table represents two-qubit CNOT gate.

Qubit	T_1 (μs)	T_2 (μs)	X (10^{-4})	Readout (10^{-2})	Qubit pair	CX (10^{-2})
Q0	51	33	4.0	4.3	[Q0, Q1]	1.484
Q1	110	105	2.0	2.2	[Q1, Q2]	0.957
Q2	114	149	3.5	2.9	[Q1, Q3]	0.671
Q3	102	201	3.9	2.0	[Q3, Q5]	1.168
Q4	107	75	2.4	3.1	[Q4, Q5]	1.091
Q5	37	72	4.2	1.2	[Q5, Q6]	0.948
Q6	107	188	6.4	2.4		

in a $2^N \times 2^N$ matrix C,

$$C_{ij} = p(i,j), \tag{C1}$$

where $p(i,j)$ is the probability of preparing state i and measuring state j. If the single-gate errors are small compared to the readout noise, this matrix perfectly maps the ideal expected results onto the measured results using a classical postprocessing of the statistics

$$p_{\text{exp}} = C p_{\text{ideal}}. \tag{C2}$$

Thus, to obtain the ideal results, we apply the inverse of C onto our measurements. All the manipulations described above are implemented in the QISKIT package [135] and used in our study.

[1] R. O. Jones, Density functional theory: Its origins, rise to prominence, and future, Rev. Mod. Phys. **87**, 897 (2015).

[2] A. Krylov, T. L. Windus, T. Barnes, E. Marin-Rimoldi, J. A. Nash, B. Pritchard, D. G. A. Smith, D. Altarawy, P. Saxe, and C. Clementi *et al.*, Perspective: Computational chemistry software and its advancement as illustrated through three grand challenge cases for molecular science, J. Chem. Phys. **149**, 180901 (2018).

[3] G. R. Schleder, A. C. M. Padilha, C. M. Acosta, M. Costa, and A. Fazzio, From DFT to machine learning: recent approaches to materials science-a review, J. Phys.: Mater. **2**, 032001 (2019).

[4] R. J. Maurer, C. Freysoldt, A. M. Reilly, J. G. Brandenburg, O. T. Hofmann, T. Björkman, S. Lebègue, and A. Tkatchenko, Advances in density-functional calculations for materials modeling, Annu. Rev. Mater. Res. **49**, 1 (2019).

[5] M. Bogojeski, L. Vogt-Maranto, M. E. Tuckerman, K.-R. Müller, and K. Burke, Quantum chemical accuracy from density functional approximations via machine learning, Nat. Commun. **11**, 1 (2020).

[6] A. T. Bell and M. Head-Gordon, Quantum mechanical modeling of catalytic processes, Annu. Rev. Chem. Biomol. Eng. **2**, 453 (2011).

[7] S. Xu and E. A. Carter, Theoretical Insights into Heterogeneous (Photo)electrochemical CO_2 Reduction, Chem. Rev. **119**, 6631 (2019).

[8] S. Hammes-Schiffer and G. Galli, Integration of theory and experiment in the modelling of heterogeneous electrocatalysis, Nat. Energy **6**, 700 (2021).

[9] D. Lee, W. Wang, C. Zhou, X. Tong, M. Liu, G. Galli, and K.-S. Choi, The impact of surface composition on the interfacial energetics and photoelectrochemical properties of $BiVO_4$, Nat. Energy **6**, 287 (2021).

[10] J. R. Weber, W. F. Koehl, J. B. Varley, A. Janotti, B. B. Buckley, C. G. V. de Walle, and D. D. Awschalom, Quantum computing with defects, Proc. Natl Acad. Sci. **107**, 8513 (2010).

[11] G. Wolfowicz, F. J. Heremans, C. P. Anderson, S. Kanai, H. Seo, A. Gali, G. Galli, and D. D. Awschalom, Quantum guidelines for solid-state spin defects, Nat. Rev. Mater. **6**, 1 (2021).

[12] Y. Cao, J. Romero, J. P. Olson, M. Degroote, P. D. Johnson, M. Kieferová, I. D. Kivlichan, T. Menke, B. Peropadre, and N. P. D. Sawaya *et al.*, Quantum chemistry in the age of quantum computing, Chem. Rev. **119**, 10856 (2019).

[13] K. Head-Marsden, J. Flick, C. J. Ciccarino, and P. Narang, Quantum information and algorithms for correlated quantum matter, Chem. Rev. **121**, 3061 (2020).

[14] B. Bauer, S. Bravyi, M. Motta, and G. Kin-Lic Chan, Quantum algorithms for quantum chemistry and quantum materials science, Chem. Rev. **120**, 12685 (2020).

[15] A. Aspuru-Guzik, A. D. Dutoi, P. J. Love, and M. Head-Gordon, Simulated quantum computation of molecular energies, Science **309**, 1704 (2005).

[16] P. J. J. O'Malley, R. Babbush, I. D. Kivlichan, J. Romero, J. R. McClean, R. Barends, J. Kelly, P. Roushan, A. Tranter, and N. Ding *et al.*, Scalable Quantum Simulation of Molecular Energies, Phys. Rev. X **6**, 031007 (2016).

[17] Y. Shen, X. Zhang, S. Zhang, J.-N. Zhang, M.-H. Yung, and K. Kim, Quantum implementation of the unitary coupled cluster for simulating molecular electronic structure, Phys. Rev. A **95**, 020501 (2017).

[18] A. Kandala, A. Mezzacapo, K. Temme, M. Takita, M. Brink, J. M. Chow, and J. M. Gambetta, Hardware-efficient variational quantum eigensolver for small molecules and quantum magnets, Nature **549**, 242 (2017).

[19] R. Santagati, J. Wang, A. A. Gentile, S. Paesani, N. Wiebe, J. R. McClean, S. Morley-Short, P. J. Shadbolt, D. Bonneau, and J. W. Silverstone *et al.*, Witnessing eigenstates for quantum simulation of Hamiltonian spectra, Sci. Adv. **4**, eaap9646 (2018).

[20] C. Hempel, C. Maier, J. Romero, J. McClean, T. Monz, H. Shen, P. Jurcevic, B. P. Lanyon, P. Love, and R. Babbush *et al.*, Quantum Chemistry Calculations on a Trapped-Ion Quantum Simulator, Phys. Rev. X **8**, 031022 (2018).

[21] I. G. Ryabinkin, T.-C. Yen, S. N. Genin, and A. F. Izmaylov, Qubit coupled cluster method: A systematic approach to quantum chemistry on a quantum computer, J. Chem. Theory Comput. **14**, 6317 (2018).

[22] A. J. McCaskey, Z. P. Parks, J. Jakowski, S. V. Moore, T. D. Morris, T. S. Humble, and R. C. Pooser, Quantum chemistry as a benchmark for near-term quantum computers, Npj Quantum Inf. **5**, 1 (2019).

[23] Z. Li, X. Liu, H. Wang, S. Ashhab, J. Cui, H. Chen, X. Peng, and J. Du, Quantum Simulation of Resonant Transitions for Solving the Eigenproblem of an Effective Water Hamiltonian, Phys. Rev. Lett. **122**, 090504 (2019).

[24] S. E. Smart and D. A. Mazziotti, Quantum-classical hybrid algorithm using an error-mitigating N-representability condition to compute the Mott metal-insulator transition, Phys. Rev. A **100**, 022517 (2019).

[25] R. Sagastizabal, X. Bonet-Monroig, M. Singh, M. A. Rol, C. C. Bultink, X. Fu, C. H. Price, V. P. Ostroukh, N. Muthusubramanian, and A. Bruno *et al.*, Experimental error mitigation via symmetry verification in a variational quantum eigensolver, Phys. Rev. A **100**, 010302 (2019).

[26] Google AI Quantum and Collaborators, Hartree-Fock on a superconducting qubit quantum computer, Science **369**, 1084 (2020).

[27] M. Metcalf, N. P. Bauman, K. Kowalski, and W. A. de Jong, Resource-efficient chemistry on quantum computers with the variational quantum eigensolver and the double unitary coupled-cluster approach, J. Chem. Theory. Comput. **16**, 6165 (2020).

[28] Y. Nam, J.-S. Chen, N. C. Pisenti, K. Wright, C. Delaney, D. Maslov, K. R. Brown, S. Allen, J. M. Amini, and J. Apisdorf *et al.*, IBM Q experience as a versatile experimental testbed for simulating open quantum systems, Npj Quantum Inf. **6**, 1 (2020).

[29] Q. Gao, H. Nakamura, T. P. Gujarati, G. O. Jones, J. E. Rice, S. P. Wood, M. Pistoia, J. M. Garcia, and N. Yamamoto, Computational investigations of the lithium superoxide dimer rearrangement on noisy quantum devices, J. Phys. Chem. A **125**, 1827 (2021).

[30] M. Rossmannek, P. K. Barkoutsos, P. J. Ollitrault, and I. Tavernelli, Quantum HF/DFT-embedding algorithms for electronic structure calculations: Scaling up to complex molecular systems, J. Chem. Phys. **154**, 114105 (2021).

[31] Y. Kawashima, E. Lloyd, M. P. Coons, Y. Nam, S. Matsuura, A. J. Garza, S. Johri, L. Huntington, V. Senicourt, and A. O. Maksymov *et al.*, Optimizing electronic structure simulations on a trapped-ion quantum computer using problem decomposition, Commun. Phys. **4**, 1 (2021).

[32] A. Teplukhin, B. K. Kendrick, S. M. Mniszewski, Y. Zhang, A. Kumar, C. F. Negre, P. M. Anisimov, S. Tretiak, and P. A. Dub, Computing molecular excited states on a D-wave quantum annealer, Sci. Rep. **11**, 1 (2021).

[33] J. J. M. Kirsopp, C. Di Paola, D. Z. Manrique, M. Krompiec, G. Greene-Diniz, W. Guba, A. Meyder, D. Wolf, M. Strahm, and D. M. Ramo *et al.*, arXiv preprint arXiv:2110.08163 (2021).

[34] M. A. Jones, H. J. Vallury, C. D. Hill, and L. C. Hollenberg, arXiv preprint arXiv:2111.08132 (2021).

[35] Z. Li, M.-H. Yung, H. Chen, D. Lu, J. D. Whitfield, X. Peng, A. Aspuru-Guzik, and J. Du, Solving quantum ground-state problems with nuclear magnetic resonance, Sci. Rep. **1**, 88 (2011).

[36] P. M. Q. Cruz, G. Catarina, R. Gautier, and J. Fernández-Rossier, Optimizing quantum phase estimation for the simulation of Hamiltonian eigenstates, Quantum Sci. Technol. **5**, 044005 (2020).

[37] I. D. Kivlichan, C. Gidney, D. W. Berry, N. Wiebe, J. McClean, W. Sun, Z. Jiang, N. Rubin, A. Fowler, A. Aspuru-Guzik, H. Neven, and R. Babbush, Improved Fault-Tolerant Quantum Simulation of Condensed-Phase Correlated Electrons via Trotterization, Quantum **4**, 296 (2020).

[38] A. Montanaro and S. Stanisic, arXiv:2006.01179 [quant-ph] (2020).

[39] A. Uvarov, J. D. Biamonte, and D. Yudin, Variational quantum eigensolver for frustrated quantum systems, Phys. Rev. B **102**, 075104 (2020).

[40] M. Motta, C. Sun, A. T. K. Tan, M. J. O'Rourke, E. Ye, A. J. Minnich, F. G. S. L. Brandão, and G. K.-L. Chan, Determining eigenstates and thermal states on a quantum computer using quantum imaginary time evolution, Nat. Phys. **16**, 205 (2020).

[41] F. Mei, Q. Guo, Y.-F. Yu, L. Xiao, S.-L. Zhu, and S. Jia, Digital Simulation of Topological Matter on Programmable Quantum Processors, Phys. Rev. Lett. **125**, 160503 (2020).

[42] L. Bassman, R. Van Beeumen, E. Younis, E. Smith, C. Iancu, and W. A. de Jong, arXiv preprint arXiv:2103.07429 (2021).

[43] L. Mineh and A. Montanaro, arXiv preprint arXiv:2108.08611 (2021).

[44] C. Powers, L. Bassman, and W. A. de Jong, arXiv preprint arXiv:2109.01619 (2021).

[45] F. T. Cerasoli, K. Sherbert, J. Sławińska, and M. B. Nardelli, Quantum computation of silicon electronic band structure, Phys. Chem. Chem. Phys. **22**, 21816 (2020).

[46] S. H. Sureshbabu, M. Sajjan, S. Oh, and S. Kais, Implementation of quantum machine learning for electronic structure calculations of periodic systems on quantum computing devices, J. Chem. Inf. Model. **61**, 2667 (2021).

[47] K. Choudhary, Quantum computation for predicting electron and phonon properties of solids, J. Phys.: Condens. Matter **33**, 385501 (2021).

[48] K. Yamamoto, D. Z. Manrique, I. Khan, H. Sawada, and D. M. Ramo, arXiv preprint arXiv:2109.08401 (2021).

[49] P. Ball, Nature.

[50] H. Ma, M. Govoni, and G. Galli, Machine learning enabled autonomous microstructural characterization in 3D samples, Npj Comput. Mater. **6**, 1 (2020).

[51] S. Endo, Z. Cai, S. C. Benjamin, and X. Yuan, Hybrid quantum-classical algorithms and quantum error mitigation, J. Phys. Soc. Jpn **90**, 032001 (2021).

[52] Y. Li and S. C. Benjamin, Efficient variational quantum simulator incorporating active error minimization, Phys. Rev. X **7**, 021050 (2017).

[53] K. Temme, S. Bravyi, and J. M. Gambetta, Error Mitigation for Short-Depth Quantum Circuits, Phys. Rev. Lett. **119**, 180509 (2017).

[54] S. Endo, S. C. Benjamin, and Y. Li, Practical Quantum Error Mitigation for Near-Future Applications, Phys. Rev. X **8**, 031027 (2018).

[55] S. Lloyd and C. Weedbrook, Quantum Generative Adversarial Learning, Phys. Rev. Lett. **121**, 040502 (2018).

[56] R. Sagastizabal, X. Bonet-Monroig, M. Singh, M. A. Rol, C. Bultink, X. Fu, C. Price, V. Ostroukh, N. Muthusubramanian, and A. Bruno *et al.*, Experimental error mitigation via symmetry verification in a variational quantum eigensolver, Phys. Rev. A **100**, 010302 (2019).

[57] J. Sun, X. Yuan, T. Tsunoda, V. Vedral, S. C. Benjamin, and S. Endo, Mitigating Realistic Noise in Practical Noisy Intermediate-Scale Quantum Devices, Phys. Rev. Appl. **15**, 034026 (2021).

[58] N. Sheng, C. Vorwerk, M. Govoni, and G. Galli, arXiv preprint arXiv:2105.04736 (2021).

[59] H. Ma, N. Sheng, M. Govoni, and G. Galli, Quantum embedding theory for strongly correlated states in materials, J. Chem. Theory Comput. **17**, 2116 (2021).

[60] J. Weber, W. Koehl, J. Varley, A. Janotti, B. Buckley, C. Van de Walle, and D. D. Awschalom, Quantum computing with defects, Proc. Natl. Acad. Sci. **107**, 8513 (2010).

[61] W. Pfaff, B. J. Hensen, H. Bernien, S. B. van Dam, M. S. Blok, T. H. Taminiau, M. J. Tiggelman, R. N. Schouten, M. Markham, and D. J. Twitchen *et al.*, Unconditional quantum teleportation between distant solid-state quantum bits, Science **345**, 532 (2014).

[62] S. Hsieh, P. Bhattacharyya, C. Zu, T. Mittiga, T. Smart, F. Machado, B. Kobrin, T. Höhn, N. Rui, and M. Kamrani *et al.*, Imaging stress and magnetism at high pressures using a nanoscale quantum sensor, Science **366**, 1349 (2019).

[63] F. Libisch, C. Huang, and E. A. Carter, Embedded correlated wavefunction schemes: Theory and applications, Acc. Chem. Res. **47**, 2768 (2014).

[64] S. Wouters, C. A. Jiménez-Hoyos, Q. Sun, and G. K.-L. Chan, A practical guide to density matrix embedding theory in quantum chemistry, J. Chem. Theory Comput. **12**, 2706 (2016).

[65] M. R. Hermes and L. Gagliardi, Multiconfigurational self-consistent field theory with density matrix embedding: The localized active space self-consistent field method, J. Chem. Theory Comput. **15**, 972 (2019).

[66] H. Q. Pham, M. R. Hermes, and L. Gagliardi, Periodic electronic structure calculations with the density matrix embedding theory, J. Chem. Theory Comput. **16**, 130 (2019).

[67] H. Ma, N. Sheng, M. Govoni, and G. Galli, First-principles studies of strongly correlated states in defect spin qubits in diamond, Phys. Chem. Chem. Phys. **22**, 25522 (2020).

[68] T. N. Lan and D. Zgid, Generalized self-energy embedding theory, J. Phys. Chem. Lett. **8**, 2200 (2017).

[69] D. Zgid and E. Gull, Finite temperature quantum embedding theories for correlated systems, New J. Phys. **19**, 023047 (2017).

[70] F. Aryasetiawan, M. Imada, A. Georges, G. Kotliar, S. Biermann, and A. I. Lichtenstein, Frequency-dependent local interactions and low-energy effective models from electronic structure calculations, Phys. Rev. B **70**, 195104 (2004).

[71] F. Aryasetiawan, J. M. Tomczak, T. Miyake, and R. Sakuma, Downfolded Self-Energy of Many-Electron Systems, Phys. Rev. Lett. **102**, 176402 (2009).

[72] T. Miyake and F. Aryasetiawan, Screened Coulomb interaction in the maximally localized Wannier basis, Phys. Rev. B **77**, 085122 (2008).

[73] H. Ma, M. Govoni, F. Gygi, and G. Galli, A finite-field approach for GW calculations beyond the random phase approximation, J. Chem. Theory Comput. **15**, 154 (2019).

[74] N. L. Nguyen, H. Ma, M. Govoni, F. Gygi, and G. Galli, Finite-Field Approach to Solving the Bethe-Salpeter Equation, Phys. Rev. Lett. **122**, 237402 (2019).

[75] T. Helgaker, P. Jorgensen, and J. Olsen, *Molecular Electronic-Structure Theory* (John Wiley & Sons, Chichester, 2014).

[76] K. D. Vogiatzis, D. Ma, J. Olsen, L. Gagliardi, and W. A. De Jong, Pushing configuration-interaction to the limit: Towards massively parallel MCSCF calculations, J. Chem. Phys. **147**, 184111 (2017).

[77] D. S. Levine, D. Hait, N. M. Tubman, S. Lehtola, K. B. Whaley, and M. Head-Gordon, CASSCF with extremely large active spaces using the adaptive sampling configuration interaction method, J. Chem. Theory Comput. **16**, 2340 (2020).

[78] A. Y. Kitaev, arXiv preprint arXiv:quant-ph/9511026 (1995).

[79] D. S. Abrams and S. Lloyd, Simulation of Many-Body Fermi Systems on a Universal Quantum Computer, Phys. Rev. Lett. **79**, 2586 (1997).

[80] D. S. Abrams and S. Lloyd, Quantum Algorithm Providing Exponential Speed Increase for Finding Eigenvalues and Eigenvectors, Phys. Rev. Lett. **83**, 5162 (1999).

[81] V. E. Elfving, B. W. Broer, M. Webber, J. Gavartin, M. D. Halls, K. P. Lorton, and A. Bochevarov, arXiv preprint arXiv:2009.12472 (2020).

[82] A. Peruzzo, J. McClean, P. Shadbolt, M.-H. Yung, X.-Q. Zhou, P. J. Love, A. Aspuru-Guzik, and J. L. O'Brien, A variational eigenvalue solver on a photonic quantum processor, Nat. Commun. **5**, 4213 (2014).

[83] M. Cerezo, A. Arrasmith, R. Babbush, S. C. Benjamin, S. Endo, K. Fujii, J. R. McClean, K. Mitarai, X. Yuan, and L. Cincio *et al.*, Variational quantum algorithms, Nat. Rev. Phys. **3**, 1 (2021).

[84] D. A. Fedorov, M. J. Otten, S. K. Gray, and Y. Alexeev, Ab initio molecular dynamics on quantum computers, J. Chem. Phys. **154**, 164103 (2021).

[85] K. Seetharam, D. Biswas, C. Noel, A. Risinger, D. Zhu, O. Katz, S. Chattopadhyay, M. Cetina, C. Monroe, and E. Demler *et al.*, arXiv preprint arXiv:2109.13298 (2021).

[86] C.-K. Lee, C.-Y. Hsieh, S. Zhang, and L. Shi, arXiv preprint arXiv:2106.10767 (2021).

[87] G. Verdon, J. Marks, S. Nanda, S. Leichenauer, and J. Hidary, arXiv preprint arXiv:1910.02071 (2019).

[88] X.-Y. Guo, S.-S. Li, X. Xiao, Z.-C. Xiang, Z.-Y. Ge, H.-K. Li, P.-T. Song, Y. Peng, K. Xu, and P. Zhang *et al.*, arXiv preprint arXiv:2107.06234 (2021).

[89] P. Jordan, J. v. Neumann, and E. Wigner, On an algebraic generalization of the quantum mechanical formalism, Ann. Math. **35**, 29 (1934).

[90] S. B. Bravyi and A. Y. Kitaev, Fermionic quantum computation, Ann. Phys. (N.Y.) **298**, 210 (2002).

[91] S. Bravyi, J. M. Gambetta, A. Mezzacapo, and K. Temme, arXiv preprint arXiv:1701.08213 (2017).

[92] J. Romero, R. Babbush, J. R. McClean, C. Hempel, P. J. Love, and A. Aspuru-Guzik, Strategies for quantum computing molecular energies using the unitary coupled cluster ansatz, Quantum Sci. Technol. **4**, 014008 (2018).

[93] J. Čížek, On the correlation problem in atomic and molecular systems. Calculation of wavefunction components in Ursell-type expansion using quantum-field theoretical methods, J. Chem. Phys. **45**, 4256 (1966).

[94] R. J. Bartlett and M. Musiał, Coupled-cluster theory in quantum chemistry, Rev. Mod. Phys. **79**, 291 (2007).

[95] H. R. Grimsley, D. Claudino, S. E. Economou, E. Barnes, and N. J. Mayhall, Is the Trotterized UCCSD ansatz chemically well-defined?, J. Chem. Theory Comput. **16**, 1 (2019).

[96] O. Higgott, D. Wang, and S. Brierley, Variational quantum computation of excited states, Quantum **3**, 156 (2019).

[97] J. R. McClean, N. C. Rubin, K. J. Sung, I. D. Kivlichan, X. Bonet-Monroig, Y. Cao, C. Dai, E. S. Fried, C. Gidney, and B. Gimby *et al.*, OpenFermion: The electronic structure package for quantum computers, Quantum Sci. Technol. **5**, 034014 (2020).

[98] S. McArdle, S. Endo, A. Aspuru-Guzik, S. C. Benjamin, and X. Yuan, Quantum computational chemistry, Rev. Mod. Phys. **92**, 015003 (2020).

[99] J. I. Colless, V. V. Ramasesh, D. Dahlen, M. S. Blok, M. E. Kimchi-Schwartz, J. R. McClean, J. Carter, W. A. de Jong, and I. Siddiqi, Computation of Molecular Spectra on a Quantum Processor with an Error-Resilient Algorithm, Phys. Rev. X **8**, 011021 (2018).

[100] G. Aleksandrowicz, T. Alexander, P. Barkoutsos, L. Bello, Y. Ben-Haim, D. Bucher, F. Cabrera-Hernández, J. Carballo-Franquis, A. Chen, and C. Chen *et al.*, Qiskit: An open-source framework for quantum computing, Accessed: Mar **16** (2019).

[101] A. Dewes, F. Ong, V. Schmitt, R. Lauro, N. Boulant, P. Bertet, D. Vion, and D. Esteve, Characterization of a Two-Transmon Processor with Individual Single-Shot Qubit Readout, Phys. Rev. Lett. **108**, 057002 (2012).

[102] F. B. Maciejewski, Z. Zimborás, and M. Oszmaniec, Mitigation of readout noise in near-term quantum devices by classical post-processing based on detector tomography, Quantum **4**, 257 (2020).

[103] P. Giannozzi, S. Baroni, N. Bonini, M. Calandra, R. Car, C. Cavazzoni, D. Ceresoli, G. L. Chiarotti, M. Cococcioni, and I. Dabo *et al.*, QUANTUM ESPRESSO: A modular and open-source software project for quantum simulations of materials, J. Phys.: Condens. Matter **21**, 395502 (2009).

[104] J. H. Skone, M. Govoni, and G. Galli, Self-consistent hybrid functional for condensed systems, Phys. Rev. B **89**, 195112 (2014).

[105] M. Govoni and G. Galli, Large scale GW calculations, J. Chem. Theory Comput. **11**, 2680 (2015).

[106] F. Gygi, Architecture of Qbox: A scalable first-principles molecular dynamics code, IBM J. Res. Dev. **52**, 137 (2008).

[107] M. Govoni, J. Whitmer, J. de Pablo, F. Gygi, and G. Galli, Code interoperability extends the scope of quantum simulations, Npj Comput. Mater. **7**, 1 (2021).

[108] Q. Sun, T. C. Berkelbach, N. S. Blunt, G. H. Booth, S. Guo, Z. Li, J. Liu, J. D. McClain, E. R. Sayfutyarova, and S. Sharma *et al.*, PySCF: the Python-based simulations of chemistry framework, Wiley Interdiscip. Rev.: Comput. Mol. Sci. **8**, e1340 (2018).

[109] M. J. Powell, in *Advances in Optimization and Numerical Analysis* (, 1994), p. 51.

[110] A. W. Cross, L. S. Bishop, J. A. Smolin, and J. M. Gambetta, arXiv preprint arXiv:1707.03429 (2017).

[111] J. C. Spall *et al.*, Multivariate stochastic approximation using a simultaneous perturbation gradient approximation, IEEE Trans. Automat. Contr. **37**, 332 (1992).

[112] N. P. Sawaya, M. Smelyanskiy, J. R. McClean, and A. Aspuru-Guzik, Error sensitivity to environmental noise in quantum circuits for chemical state preparation, J. Chem. Theory Comput. **12**, 3097 (2016).

[113] S. McArdle, X. Yuan, and S. Benjamin, Error-Mitigated Digital Quantum Simulation, Phys. Rev. Lett. **122**, 180501 (2019).

[114] Y. Shee, P.-K. Tsai, C.-L. Hong, H.-C. Cheng, and H.-S. Goan, arXiv preprint arXiv:2110.04112 (2021).

[115] V. E. Elfving, M. Millaruelo, J. A. Gámez, and C. Gogolin, Simulating quantum chemistry in the seniority-zero space on qubit-based quantum computers, Phys. Rev. A **103**, 032605 (2021).

[116] M. Otten and S. K. Gray, Accounting for errors in quantum algorithms via individual error reduction, Npj Quantum Inf. **5**, 1 (2019).

[117] A. Strikis, D. Qin, Y. Chen, S. C. Benjamin, and Y. Li, Learning-based quantum error mitigation, PRX Quantum **2**, 040330 (2021).

[118] P. Czarnik, A. Arrasmith, P. J. Coles, and L. Cincio, Error mitigation with Clifford quantum-circuit data, Quantum **5**, 592 (2021).

[119] A. Zlokapa and A. Gheorghiu, arXiv preprint arXiv:2005.10811 (2020).

[120] J. Rogers, G. Bhattacharyya, M. S. Frank, T. Jiang, O. Christiansen, Y.-X. Yao, and N. Lanatà, arXiv preprint arXiv:2111.08814 (2021).

[121] A. Kandala, K. Temme, A. D. Córcoles, A. Mezzacapo, J. M. Chow, and J. M. Gambetta, Error mitigation extends the computational reach of a noisy quantum processor, Nature **567**, 491 (2019).

[122] E. F. Dumitrescu, A. J. McCaskey, G. Hagen, G. R. Jansen, T. D. Morris, T. Papenbrock, R. C. Pooser, D. J. Dean, and P. Lougovski, Cloud Quantum Computing of an Atomic Nucleus, Phys. Rev. Lett. **120**, 210501 (2018).

[123] B. Fauseweh and J.-X. Zhu, Digital quantum simulation of non-equilibrium quantum many-body systems, Quantum Inf. Proc. **20**, 1 (2021).

[124] A. He, B. Nachman, W. A. de Jong, and C. W. Bauer, Zero-noise extrapolation for quantum-gate error mitigation with identity insertions, Phys. Rev. A **102**, 012426 (2020).

[125] T. Giurgica-Tiron, Y. Hindy, R. LaRose, A. Mari, and W. J. Zeng, in *2020 IEEE International Conference on Quantum Computing and Engineering (QCE)* (IEEE, 2020), p. 306.

[126] J. J. Wallman and J. Emerson, Noise tailoring for scalable quantum computation via randomized compiling, Phys. Rev. A **94**, 052325 (2016).

[127] S. Tomkins and R. de Sousa, in *2020 IEEE International Conference on Quantum Computing and Engineering (QCE)* (IEEE, 2020), p. 413.

[128] J. Lee, W. J. Huggins, M. Head-Gordon, and K. B. Whaley, Generalized unitary coupled cluster wave functions for quantum computation, J. Chem. Theory Comput. **15**, 311 (2018).

[129] I. G. Ryabinkin, T.-C. Yen, S. N. Genin, and A. F. Izmaylov, Qubit coupled cluster method: A systematic approach to quantum chemistry on a quantum computer, J. Chem. Theory Comput. **14**, 6317 (2018).

[130] N. P. Bauman, E. J. Bylaska, S. Krishnamoorthy, G. H. Low, N. Wiebe, C. E. Granade, M. Roetteler, M. Troyer, and K. Kowalski, Downfolding of many-body Hamiltonians using active-space models: Extension of the sub-system embedding sub-algebras approach to unitary coupled cluster formalisms, J. Chem. Phys. **151**, 014107 (2019).

[131] M. Metcalf, N. P. Bauman, K. Kowalski, and W. A. De Jong, Resource-efficient chemistry on quantum computers with the variational quantum eigensolver and the double unitary coupled-cluster approach, J. Chem. Theory. Comput. **16**, 6165 (2020).

[132] D. A. Fedorov, Y. Alexeev, S. K. Gray, and M. Otten, arXiv preprint arXiv:2109.12652 (2021).

[133] J. Liu and L. Cheng, Unitary coupled-cluster based self-consistent polarization propagator theory: A quadratic unitary coupled-cluster singles and doubles scheme, J. Chem. Phys. **155**, 174102 (2021).

[134] K. J. M. Korol, K. Choo, and A. Mezzacapo, arXiv preprint arXiv:2111.08090 (2021).

[135] A. Asfaw, A. Corcoles, L. Bello, Y. Ben-Haim, M. Bozzo-Rey, S. Bravyi, N. Bronn, L. Capelluto, A. C. Vazquez, and J. Ceroni *et al.*, Learn quantum computation using QISKIT (2020).